A broadband method for the measurement of the surface impedance of thin films at microwave frequencies

J. C. Booth, Dong Ho Wu, and Steven M. Anlage
Center for Superconductivity Research, Department of Physics, University of Maryland, College Park, Maryland 20742-4111

(Received 11 February 1994; accepted for publication 15 March 1994)

We present a new technique to measure the complex surface impedance of the mixed state of superconducting thin films over the broad frequency range 45 MHz–20 GHz. The surface impedance is extracted from measurements of the complex reflection coefficient made on the film using a vector network analyzer. The technique takes advantage of a special geometry in which the self-fields from currents flowing in the film are everywhere parallel to the film surface, making it an ideal configuration in which to study vortex dynamics in superconductors. The broadband nature of the measurement system allows us to explore a region of magnetic field–temperature–frequency parameter space of superconductors previously inaccessible with other measurement techniques. The power of the technique is illustrated by measurements on thin films of the high temperature superconductor $YBa_2Cu_3O_{7-\delta}$.

I. INTRODUCTION

Microwave surface impedance measurements provide a powerful tool for studying the electrodynamic properties of conductors and dielectrics. A compelling subject for such measurements is the mixed state of type II superconductors, where the motion of quantized magnetic vortices is of interest for both practical and fundamental reasons. Surface impedance measurements of superconductors carried out over a broad range of experimental parameters (such as temperature, magnetic field strength, current density, and frequency) can yield a great deal of valuable information about vortex dynamics in superconductors and aid considerably in the development of a complete theory of vortex motion. The technique we describe here has been developed specifically for the measurement of vortex dynamics at microwave frequencies, although the method is applicable to a variety of other systems.

The information obtained from microwave measurements about vortex motion is important for many technological applications of superconductivity, as well as for fundamental reasons. Surface impedance measurements can, for example, be used to characterize the pinning forces and activation barriers which prevent dissipative vortex motion in both rf and dc applications of superconductivity. Of fundamental interest is the question of what general laws govern vortex motion in superconductors. For instance, it is not clear if single particle phenomenological models[1,2] can adequately describe vortex motion at microwave frequencies. Alternative theories of vortex motion predict the existence of vortex core excitations and unusual optical activity,[3] which should be observable in surface impedance measurements. In addition, the search for collective properties of the vortex state, such as phase transitions between a glassy and liquid state,[4] also provide motivation for a careful study of vortex dynamics in superconductors using high frequency techniques.

Most conventional microwave measurements of the surface impedance rely on resonance methods, in which the sample forms all or part of a resonant structure.[5–7] While such techniques can potentially provide a very sensitive means of studying the surface impedance as a function of temperature or magnetic field, they are necessarily limited to at most a few discrete frequency points, and therefore cannot provide much information on how the surface impedance varies with frequency. The inability of resonance techniques to measure any frequency dependence can be a serious drawback when interpreting experimental results on vortex dynamics since it is often possible to describe results obtained at a single frequency by an uninformative parametrization of the data. The behavior of the system at many different frequencies will provide a much more stringent test of any theoretical model. More broadband techniques, such as waveguide transmission measurements,[8,9] can be applied to investigate the frequency dependence of the vortex state, but such measurements are still limited to the operating frequency range of the waveguide used, and have the disadvantage that it can be quite difficult to extract the surface impedance from the experimentally measured quantities.[10]

In this paper we describe a new nonresonant experimental technique which extends the measurement of the surface impedance of superconducting thin films to arbitrary frequencies in the rf and microwave range (45 MHz–20 GHz). Measurements at lower frequencies can be accomplished using other methods.[11–13] Our technique employs a vector network analyzer to measure the complex reflection coefficient (S_{11}) of a thin film which forms and electrical short across the end of a coaxial cable. Once the complex reflection coefficient is measured, standard transmission line theory is used to extract the complex surface impedance of the film from S_{11}. The measurement also takes advantage of a special geometry in which the sample forms a thin disc between the inner and outer conductors of the coaxial cable (see Fig. 1, inset). The use of such a measurement geometry—also referred to as a Corbino disk[14] geometry—means that currents in the film flow in the radial direction, producing magnetic fields only in the azimuthal direction, everywhere parallel to the surface of the film. The effects of the edges of the film are therefore effectively eliminated in the Corbino geometry

 0034-6748/94/65(6)/2082/9/$6.00

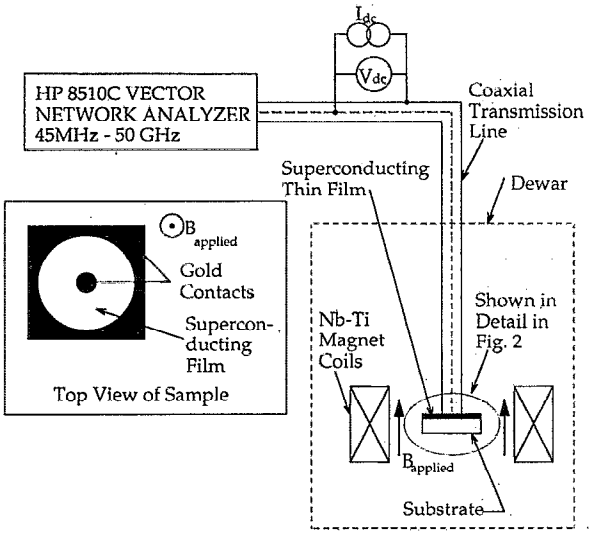

FIG. 1. Schematic diagram of reflection measurement apparatus. The coaxial cable can also be biased with an external dc current. Inset: diagram showing gold contacts as evaporated on the superconducting film. A pressure contact is made between the contacts and the coaxial transmission line.

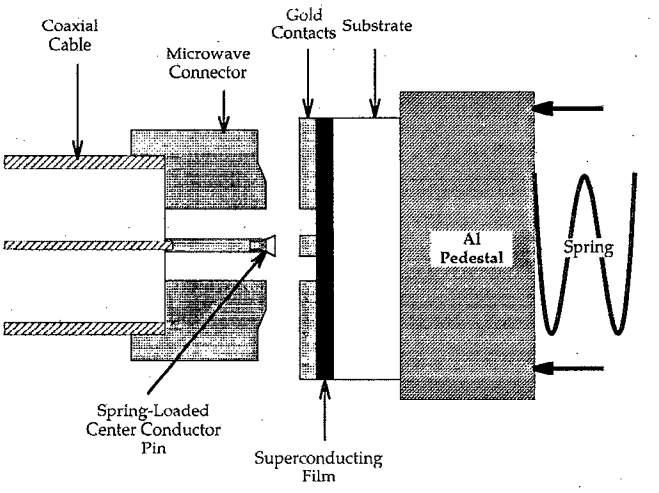

FIG. 2. Detailed view of thin film/connector interface, just prior to contact. Pressure is exerted on the aluminum pedestal by a spring in order to maintain contact between the film and connector throughout the temperature range.

(compare with a rectangular or microbridge geometry, where self fields due to the current can be perpendicular to the film surface, particularly at the edges). This geometry is particularly beneficial when studying vortex dynamics, since the sample edge contribution to the creation and/or pinning[15] of vortices has been eliminated. An additional advantage of our technique is that it allows for the surface impedance to be determined over a wide range of experimental parameters, including temperature, magnetic field, frequency, rf power, and dc bias current.

This measurement technique developed out of the historical use of the Corbino geometry for dc transport measurements.[14] Bluzer and collaborators[16] used the Corbino geometry to measure time-domain picosecond quasiparticle dynamics in zero field in low- and high- T_c superconducting films. We have adapted their technique to the frequency domain, and to the study of vortex dynamics and quasiparticle processes in superconductors.

The details of our measurement of the experimentally relevant quantity, the reflection coefficient, are described in Sec. II below. The method by which the effective surface impedance (Z_s^{eff}) is extracted from the measured reflection coefficient is covered in Sec. III, while Sec. IV describes the necessary calibration procedures and discusses the errors involved with the measurement. Section V then demonstrates the usefulness and power of the technique by presenting a broad range of experimental data on the temperature, magnetic field, and frequency dependence of Z_s^{eff} of $YBa_2Cu_3O_{7-\delta}$ (YBCO) thin films.

II. EXPERIMENTAL METHOD

Figure 1 shows a schematic representation of our experimental configuration. The thin film under study is used to terminate a coaxial transmission line, and the complex reflection coefficient S_{11} is measured over the continuous frequency range 45 MHz–20 GHz using a Hewlett–Packard HP8510C vector network analyzer. The network analyzer is operated in step sweep mode to ensure phase coherence at each frequency point. Related experimental techniques use reflection coefficient measurements to obtain the complex dielectric constant of liquids[17,18] and solids[19,20] at room temperature. In our case, the dependence of the reflection coefficient on temperature, magnetic field, and frequency is of primary interest.

A detailed diagram of the coaxial cable/film interface is shown in Fig. 2. Gold contacts a few thousand angstroms thick are evaporated through a washer-shaped shadow mask to form inner and outer electrical contacts on the film (see inset, Fig. 1). The portion of the film exposed between the contacts forms the Corbino disc proper, the inner and outer diameters of which are approximately 0.020 and 0.066 in., respectively. Electrical contact is made to the inner and outer conductors of the coaxial cable through a modified microwave connector.[21] Direct contact is made between the outer conductor of the connector and the outer contact of the film, while contact is made between the inner contact of the film and the inner conductor of the cable by means of a small pin inserted into the connector center conductor. Contact is maintained as the temperature is changed by means of an aluminum pedestal and spring assembly which apply pressure to the backside of the substrate. Such a contact can reliably hold from room temperature to 4.2 K, although the contact resistance between the connector and the film changes somewhat over this large temperature range. These changes in contact resistance with temperature are small enough to be neglected over most temperature ranges of interest (for example, between 70 and 100 K, the change in the dc contact resistance is approximately 50 mΩ/□, which is below the resolution limit of the microwave measurement).

In order to align the contacted film with the microwave connector properly, a special alignment jig is used to position the sample on the aluminum pedestal. Once the film is correctly positioned, the entire film/pedestal assembly[16] is loaded into a copper housing (not shown in Figs. 1 and 2),

which also accepts the microwave connector, and ensures that the contacts on the film align with the connector as shown in Fig. 2.

The sample is connected to the HP8510C network analyzer by means of an 0.086 in. o.d. copper coaxial transmission line,[22] which supports only the TEM mode up to 60 GHz. For our magnetic field dependence study, the transmission line must be approximately 3 m long in order to reach a Nb–Ti superconducting magnet (see Fig. 1). In this case, the attenuation due to such a long transmission line contributes to the upper limit of approximately 20 GHz on the highest measurable frequency of the measurement system.

In the Corbino disk geometry the rf currents flow in the radial direction, and the rf current density in the film is proportional to $1/r$, where r is the distance from the center of the Corbino ring. The rf current density also depends on the film thickness and the rf power supplied by the source (which may be varied from $+15$ to -15 dBm). As an example, for a 1000 Å thick film and an applied rf power of 10 dBm, and assuming the current density is uniform throughout the film thickness, the peak current density in the film is approximately 1×10^4 A/cm^2. In most cases, the actual rf power at the sample is considerably less (due to attenuation in the coaxial cable), so that this current density may be considered to be an upper bound.

In addition to measurements at rf and microwave frequencies, this technique also allows for 2-point dc measurements to be performed. A dc bias current is applied to the coaxial cable (see Fig. 1), and the resulting voltage drop between the inner and outer conductors of the coaxial cable is measured at the location of the network analyzer (an rf choke internal to the HP8510C test set protects the high frequency detectors from the dc current). This ability to make dc measurements simultaneous with the high frequency measurements allows us to compare the high frequency response with the more conventional dc behavior.

III. DATA ANALYSIS

In order to interpret our experimental data on conductors, it is necessary to extract the surface impedance Z_s from our measurements of the reflection coefficient. The reflection coefficient S_{11} is related to the load impedance Z_L of the sample by the simple formula

$$S_{11}=\frac{Z_L-Z_0}{Z_L+Z_0}, \tag{1}$$

where Z_0 is the characteristic impedance of the coaxial transmission line (assumed to be 50 Ω and real). The reflection coefficient is therefore a complex, dimensionless quantity which measures the impedance mismatch between the transmission line and the load, and is bounded in magnitude between 0 and 1.

The load impedance Z_L in Eq. (1) is the ratio of the total voltage across the Corbino disc to the total current flowing through the disc. This quantity depends on the dimensions of the Corbino disc, and assuming the presence of only the TEM mode, can be expressed in terms of the surface impedance Z_s of the film as

$$Z_L=\Gamma Z_s. \tag{2}$$

The scale factor Γ in this expression simply relates the "ohmic" impedance $Z_{IV}=V/I$, and the field impedance $Z_{\text{field}}=E_r/H_\phi$ for the TEM mode in a coaxial system (here V and I represent the voltage and current, respectively, across the coaxial cable, while E_r and H_ϕ represent the electric and magnetic fields, respectively, within the coaxial cable). The surface impedance Z_s of the film is simply the field impedance Z_{field} evaluated at the surface of the film. For a coaxial system of inner radius a and outer radius b we obtain[23] $\Gamma=\ln(b/a)/2\pi$.

Once the reflection coefficient S_{11} of the sample has been measured, one can obtain the surface impedance simply from Eqs. (1) and (2). If the load impedance Z_L of the sample is small compared to Z_0 (which is normally the case for conductors), then evaluation of the geometric factor Γ (with $2a=5.08\times10^{-4}$ m and $2b=1.68\times10^{-3}$ m) yields the following approximate relationship between changes in the reflection coefficient and changes in the surface impedance:

$$\delta|Z_s|\approx(131.6\ \Omega)\ \delta|S_{11}|. \tag{3}$$

Our measurement resolution for changes in $|S_{11}|$ at 1 GHz is approximately 0.0005, implying a resolution for changes in the surface impedance of approximately 66 mΩ at this frequency.

For comparison, the surface impedance of a bulk metallic sample in the local limit is given by

$$Z_s^\infty=\sqrt{\frac{i\mu_0\omega}{\sigma}}, \tag{4}$$

where $\sigma=1/\tilde{\rho}$ is the conductivity of the material, which is, in general, complex ($\sigma=\sigma_1-i\sigma_2$). For a numerical example, consider the superconductor $YBa_2Cu_3O_{7-\delta}$ (YBCO), which in the normal state just above T_c has a resistivity $\rho_n\sim100$ μΩ cm. With a conductivity that is completely real, evaluation of Eq. (4) at a frequency of 1 GHz gives $Z_s\sim(1+i)$ 62.8 mΩ, which is comparable in magnitude to the sensitivity limit of our measurement calculated above. This example illustrates the limited sensitivity of the measurement system for bulk metallic samples, and means that the effective surface impedance of our samples must be somehow enhanced, particularly in the superconducting state, for our technique to be useful. This is accomplished in practice by working with thin samples, where the measured surface impedance is increased due to finite film thickness effects.[24–26] The use of thin films, combined with large external magnetic fields and temperatures near T_c, provides more than adequate enhancement of the effective surface impedance for meaningful measurements with this technique.

The effective surface impedance which one measures for a film of thickness t_0 is given by

$$Z_s^{\text{eff}}=Z_s^\infty\coth(kt_0), \tag{5}$$

where Z_s^∞ is the surface impedance of a bulk sample [Eq. (4)], and $k=(i\mu_0\omega\sigma)^{1/2}$ is the complex propagation constant in the film. [When the film is in the normal state, $k=(1+i)/\delta$, where δ is the normal metal skin depth; at temperatures much below T_c the propagation constant reduces to

$k \sim 1/\lambda$, where λ is the superconductor magnetic penetration depth.] The expression in Eq. (5) implicitly assumes that the fields are zero at the backside of the film. Note also that Eq. (5) reduces to the bulk expression when the film thickness $t_0 \to \infty$.

Equation (5) can often be further simplified when applied to thin metallic or superconducting samples. If the argument of the hyperbolic cotangent function is small (true when the film thickness $t_0 \ll \delta, \lambda$) we may approximate $\coth(x)$ by $1/x$, and obtain the following remarkably simple expression for the effective surface impedance of a thin film, valid as long as $|k| t_0 \ll 1$:

$$Z_s^{\text{eff}} \approx \frac{\tilde{\rho}}{t_0} \quad (\text{for } |k| t_0 \ll 1). \tag{6}$$

Using the normal state resistivity for YBCO given above, and a film thickness of $t_0 = 1000$ Å, Eq. (6) yields $Z_s^{\text{eff}} \approx 10\ \Omega$ in the normal state, just above T_c. Thus, the effective surface resistance of a thin film is considerably enhanced relative to its infinite thickness value. In the superconducting state, when $T \ll T_c$, the effective surface impedance is dominated by the kinetic inductance of the film: $Z_s^{\text{eff}} \sim \mu_0 \omega \lambda^2(T)/t_0$, which is enhanced by a factor $\lambda(T)/t_0$ compared to the bulk value in the same limit.

Note that as a result of Eqs. (2) and (6) the measured quantity Z_L^{eff} is directly related to the complex bulk resistivity $\tilde{\rho}$ of the sample, which is a fundamentally interesting quantity. Many theories of vortex dynamics give explicit expressions for $\tilde{\rho}(B,T,\omega)$, making comparisons between our experimental data and theory straightforward. We believe that one of the main utilities of our technique is the fact that we can directly measure the bulk complex resistivity of a metallic or superconducting material.

Yet another consequence of Eq. (6) is that in the normal state, where $\tilde{\rho}$ is completely real, we expect $\text{imag}\{Z_s^{\text{eff}}\} \to 0$, in contrast to the bulk case, where $\text{imag}\{Z_s^{\infty}\} = \text{real}\{Z_s^{\infty}\}$ in the normal state. These qualitative features can be seen in Figs. 3(a) and 3(b), which show the temperature dependence of Z_s^{eff} of a YBCO thin film in zero applied magnetic field. This data will be discussed in more detail in Sec. V.

IV. CALIBRATION AND ERROR ANALYSIS

The expression for the reflection coefficient given by Eq. (1) is valid only if the measurement is performed directly at the location of the impedance discontinuity. In practice, the experimentally measured reflection coefficient will include effects due to the intervening transmission line, connectors, etc., which are necessary to perform a practical measurement. These effects become particularly important at higher frequencies, where the wavelength of the measurement signal is much smaller than the dimensions of the system. In what follows we will first discuss the calibration procedures used to minimize the systematic errors involved in our measurement of the reflection coefficient. This will be followed by a description of the measurement errors, which include random errors and any remaining systematic errors resulting from an imperfect calibration. Finally, we will address the influence of the substrate on our measurement of Z_s^{eff}.

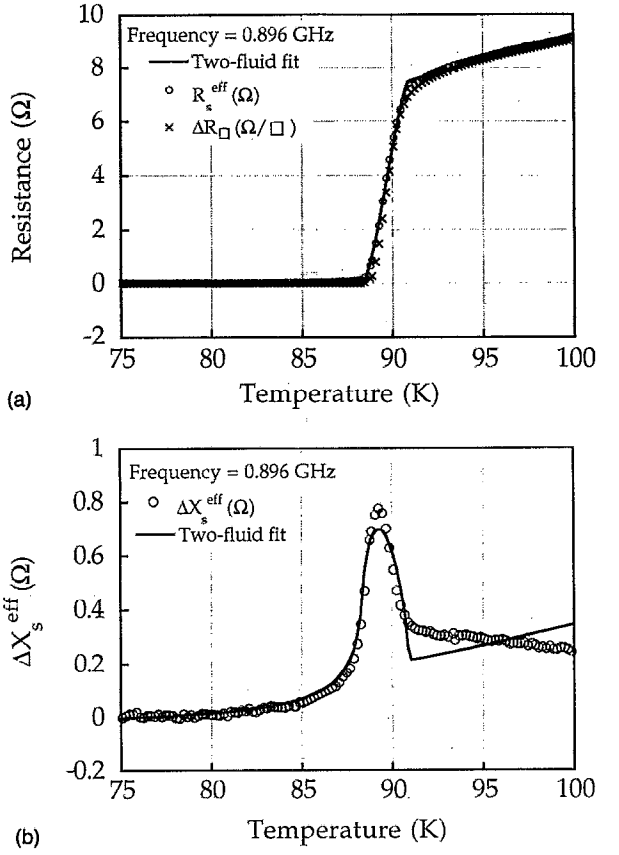

FIG. 3. Temperature dependence of the (a) real and (b) imaginary parts of the effective surface impedance for a 1000 Å thick YBCO film at a frequency of 0.896 GHz. The solid lines represent a fit to a modified two-fluid model. Also shown is the temperature dependence of the dc sheet resistance (×'s) measured simultaneously with the rf data.

A. Calibration

Our measurement of the reflection coefficient S_{11}^{actual} is in practice corrupted by attenuation and multiple reflections in the coaxial cable system, as well as by errors in the detection apparatus. These effects can be accounted for and eliminated from the data by means of a set of calibrations applied to the measured reflection coefficient S_{11}^{meas}. A general expression for the measured reflection coefficient (S_{11}^{meas}) in terms of the actual reflection coefficient (S_{11}^{actual}) can be obtained using microwave network theory[27] and is given by

$$S_{11}^{\text{meas}} = E_D + \frac{E_R S_{11}^{\text{actual}}}{1 - E_S S_{11}^{\text{actual}}}. \tag{7}$$

Here E_D, E_R, and E_S are complex error coefficients that completely characterize the detection apparatus/transmission line system. The error coefficient E_D is the directivity, which arises from the imperfect nature of the directional couplers in the test set of the network analyzer, and from reflections due to connectors in the system. These effects result in a small "leakage" of the signal from the source directly into the detectors, by-passing the load altogether. The effect of this error is easily seen by considering a reflectionless load ($S_{11}^{\text{actual}} = 0$) in Eq. (7), which shows that the measured reflection coefficient is entirely due to the leakage signal in this

limit. We find that the value of E_D has no systematic dependence on frequency, and has a magnitude bounded by approximately 0.1 for the systems used here.

The error term E_R is called the reflection tracking, and corrects principally for the attenuation and phase delay introduced by the transmission line. For a system consisting of simply a load at the end of a transmission line of length l, and for which E_D and E_S are zero, one would obtain $S_{11}^{\text{meas}}=e^{-2\gamma l}S_{11}^{\text{actual}}$, where γ is the complex propagation constant of the transmission line ($\gamma=\alpha+i\beta$, where α is the attenuation constant of the transmission line, and β is the phase constant). Comparison with Eq. (7) shows that the error coefficient E_R would be given by $E_R=e^{-2\gamma l}$ for this simple case. In practice, one finds that the frequency dependence of E_R strongly resembles $e^{-2\gamma l}$, with α increasing roughly as $\omega^{1/2}$, and $\beta=\omega/v_{\text{phase}}$, where v_{phase} is the phase velocity in the transmission line. The magnitude of E_R is close to 1 at low frequencies (indicating little attenuation), and decreases to approximately 0.1 at the high frequency limit of 20 GHz (which implies much stronger attenuation).

The third error term E_S is referred to as the source match, which arises due to the re-reflection of a portion of the signal at the measurement port, caused by the slight impedance mismatch between the detectors and the transmission line. This re-reflected signal interferes with the incident signal at the load, adding a small error to the incident signal. Since the reflection coefficient is defined as the ratio of the reflected signal to the incident signal, this error will also affect the reflection coefficient. Like E_D, the source match error coefficient shows no systematic dependence on frequency, and is also bounded in magnitude also by approximately 0.1.

The three error coefficients described above are all frequency dependent. It is possible to ascertain values for all three error coefficients at each frequency point of interest through a calibration procedure involving the measurement of three standards for which S_{11}^{actual} is known. As pointed out previously, by measuring a standard for which $S_{11}^{\text{actual}}=0$, one can directly measure the error coefficient E_D. In practice, one uses a standard short ($S_{11}^{\text{actual}}=-1$), a standard open ($S_{11}^{\text{actual}}=+1$), and a matched load ($S_{11}^{\text{actual}}=0$) to fully calibrate the system, although one can in principle use as a standard any load for which S_{11}^{actual} vs frequency is known. Once values for all three error coefficients are obtained (at each frequency point of interest), Eq. (7) can be inverted to calculate S_{11}^{actual} given S_{11}^{meas} and E_D, E_R, and E_S. This calibration procedure involving the measurement of three known standards is performed at room temperature prior to every measurement. Since our measurement makes use of a modified microwave connector to contact the sample, the calibrations are performed using this same connector, *directly at the location of the sample*. With an accurate calibration, the inversion of Eq. (7) should yield the actual reflection coefficient of the load described by Eq. (1).

B. Measurement errors

The inverse of Eq. (7) gives an expression for S_{11}^{actual} in terms of S_{11}^{meas} and the three error coefficients described above. Labeling this expression for S_{11}^{actual} as the corrected reflection coefficient S_{11}^{correct} gives

$$S_{11}^{\text{correct}}=\frac{(S_{11}^{\text{meas}}-E_D)}{E_R+E_S(S_{11}^{\text{meas}}-E_D)}. \tag{8}$$

Any error in the experimentally determined reflection coefficient, $\Delta S_{11}^{\text{correct}}$, is therefore a result of errors in the four experimentally measured quantities: $\Delta S_{11}^{\text{meas}}$, ΔE_D, ΔE_R, and ΔE_S. One obvious disadvantage of the need to perform the calibration described above is the propagation of errors. Instead of just one (complex) measured quantity, we now have four, each with its own associated uncertainty.

The measurement errors that occur in S_{11}^{correct} may be classified as either random or systematic. The random errors in S_{11}^{correct} are due solely to the random errors in the measured reflection coefficient S_{11}^{meas}. These errors may be estimated from the standard deviation obtained by performing a series of measurements on the system in the same state. The resulting upper bound for $\Delta S_{11}^{\text{meas}}$ is

$$\Delta|S_{11}^{\text{meas}}|\approx 2\times 10^{-4}. \tag{9}$$

There is no overall frequency dependence for the random errors $\Delta S_{11}^{\text{meas}}$ over our entire accessible frequency range (45 MHz–20 GHz). However, this is not true for the corresponding random errors in $\Delta S_{11}^{\text{correct}}$, since the errors in S_{11}^{meas} must be propagated through Eq. (8) to obtain the errors in S_{11}^{correct}. Such an analysis shows that at low frequencies ($\leq$2 GHz), the random errors in S_{11}^{correct} are on the order of 5×10^{-4}, while at the highest measurable frequencies (20 GHz), the random errors in S_{11}^{correct} approach approximately 2×10^{-3}. The fact that the measurement is more accurate at lower frequencies is due in part to the increased attenuation of the measurement signal at higher frequencies. These values for $\Delta S_{11}^{\text{correct}}$ determine the (frequency dependent) resolution of the measurement system, the smallest change in S_{11}^{correct} that can be observed which is statistically significant. This is also the theoretical limit of the accuracy of the system, in the absence of any systematic errors.

In practice, the accuracy of the measurement system is limited by systematic errors generated by inaccuracies in the measured values of the error coefficients E_D, E_R, and E_S. These errors are, in general, much harder to quantify than the random errors discussed above. Since E_D, E_R, and E_S are measured in the same way as S_{11}^{meas}, the uncertainty in their values is at least as large as $\Delta S_{11}^{\text{meas}}$. In addition, since the calibration is performed at room temperature, and the measurements on superconductors are made at much lower temperatures, changes in the attenuation and phase velocity of the transmission line also contribute to errors in the values of the error coefficients.[28] In order to reduce the effects of these systematic errors as much as possible, we exploit the fact that we know what the reflection coefficient of a superconductor should look like at low temperatures. This enables us to replace one of the three standards used for calibration by this "reference state" of the sample, and effectively recalibrate the system at low temperatures.

From the discussion of Sec. IV A we expect the error coefficient E_R to depend most strongly on the temperature of the transmission line, since this error coefficient corrects for

the attenuation and delay introduced by the transmission line. We therefore make the explicit assumption that the remaining error coefficients E_S and E_D do *not* change as the transmission line is cooled, and use the values for these error coefficients obtained from the room temperature calibration, along with the measured value of the reflection coefficient in our reference state, to calculate a new, more accurate value for E_R. This new value of E_R is then used in Eq. (8) over the rest of the range of the measurement. While this procedure cannot eliminate all systematic errors arising from the calibration, it does reduce such errors to an acceptable level, as will be shown in Sec. V.

C. Substrate effects

Because we make use of thin samples in order to enhance our measured value of Z_s^{eff}, we expect to encounter errors due to the transmission of radiation through the film and into the substrate if the thickness of the film under study is made sufficiently small. In order to estimate the influence of such effects on our measurements, it is necessary to calculate the applicable corrections to Eq. (5) that result from allowing a nonzero value for the fields within the substrate. A simple analysis involving TEM waves only[29] yields the following expression for the effective surface impedance of a film of thickness t_0 backed by a substrate that has a field impedance Z_s^{sub}:

$$Z_s^{\text{eff}}=\left(Z_s^{\infty}\coth(kt_0)+\frac{(Z_s^{\infty})^2}{Z_s^{\text{sub}}}\right)\Bigg/\left(1+\frac{Z_s^{\infty}\coth(kt_0)}{Z_s^{\text{sub}}}\right). \tag{10}$$

Here again Z_s^{∞} is the surface impedance of a bulk sample, and k is the complex propagation constant, as in Eq. (5). One can think of Z_s^{sub} as an effective substrate impedance that includes the effect of everything that lies behind the film, which for our geometry would include the aluminum pedestal. Note that this expression for Z_s^{eff} reduces to Eq. (5) when $Z_s^{\text{sub}}\to\infty$. Unlike Eq. (5), however, this expression gives $Z_s^{\text{eff}}=Z_s^{\text{sub}}$ as $t_0\to 0$. Under conditions where $kt_0\ll 1$ [the same assumptions that led to Eq. (6)], this expression simplifies to

$$Z_s^{\text{eff}}\approx\frac{\tilde{\rho}/t_0}{1+[(\tilde{\rho}/t_0)/Z_s^{\text{sub}}]}\quad(|k|t_0\ll 1). \tag{11}$$

This expression clearly shows the conditions under which the influence of the substrate is important: when the effective impedance of the film is comparable to the impedance of the substrate. For a low-loss dielectric substrate, the field impedance is given by $Z_s^{\text{sub}}=377\ \Omega/\sqrt{\epsilon_r}$, and assuming a value of $\epsilon_r\approx 26$ for $LaAlO_3$ gives $|Z_s^{\text{sub}}|\approx 74\ \Omega$. Making use of the YBCO example introduced previously in Sec. III and the above estimate for Z_s^{sub} shows that the corrections to Z_s^{eff} are most significant when the film is in the normal state, where the value of Z_s^{eff} is modified by approximately 10%. Note, however, that Eq. (11) also implies that when the film is fully superconducting, the corrections due to the substrate are essentially negligible, even for a very thin film.

V. SURFACE IMPEDANCE OF $YBa_2Cu_3O_{7-\delta}$

To illustrate the validity and usefulness of our experimental technique, we present here a wide range of results on thin YBCO films. We first show the temperature dependence of Z_s^{eff} at a fixed frequency in zero magnetic field, and demonstrate that our results are in agreement with dc measurements and the predictions of a modified two-fluid model. We then present new data on the magnetic field dependence of Z_s^{eff} at the same frequency to illustrate the ability of the technique to measure properties of the vortex state. This is followed by an example of the frequency dependence of Z_s^{eff} in zero magnetic field over the continuous frequency range 45 MHz–20 GHz, which illustrates the unique ability of our technique to directly measure the frequency dependence of the surface impedance of superconducting thin films in the microwave regime.

A. Zero-field temperature dependence

To verify that our technique can accurately measure the effective surface impedance of thin films, we first investigate the temperature dependence of Z_s^{eff} for a YBCO film in zero magnetic field at a single measurement frequency. We expect the YBCO system to be well described by a simple two-fluid model in the temperature range near T_c. Figures 3(a) and 3(b) show our measured values of the real and imaginary parts of Z_s^{eff} vs temperature for a 1000 Å thick YBCO film at a frequency of 0.896 GHz. The error coefficient E_R is calculated as described in Sec. IV B by making use of a reference state at 75 K, where the load impedance is dominated by the kinetic inductance of the film. Figure 3(a) shows, in addition to the 0.896 GHz data, the change in the dc sheet resistance ($\Delta R_{\square}$) vs temperature. Note that the dc sheet resistance is by definition ρ_{dc}/t_0 (t_0 is the film thickness), which is the limiting form of Z_s^{eff} in the normal state, given by Eq. (6). The excellent agreement between the dc and microwave measurements provides an independent check on the accuracy of the high-frequency measurement.

Also shown in Figs. 3(a) and 3(b) are the results of a fit to a modified two-fluid model, which uses the standard two-fluid conductivity $\sigma=\sigma_1-i\sigma_2$ in Eq. (10) to calculate $Z_s^{\text{eff}}(T)$. The model is modified to take into account the width of the superconducting transition by averaging Z_s^{eff} over a Gaussian distribution of T_c's, in order to more accurately describe our data. From such a fit we obtain the following parameters: $\Delta T_c=1.1$ K, $\lambda(0)=5300$ Å, $\rho(T_c)=74\ \mu\Omega$ cm. The relatively large values for $\lambda(0)$ and ΔT_c are probably due to inferior film quality and sample degradation during processing. More recent, higher quality samples yield smaller values for $\lambda(0)$. Here we have used Eq. (10) to calculate Z_s^{eff}, so it is necessary to include values for the real and imaginary parts of the effective substrate impedance Z_s^{sub} in the calculation.[29] We find that Z_s^{eff} is relatively insensitive to the values of Z_s^{sub}, with the exception of the imaginary part of Z_s^{eff} in the normal state. This is expected since the quantity $\tilde{\rho}/t_0$ is completely real in the normal state, and Eq. (10) implies that imag$\{Z_s^{\text{eff}}\}$ will depend strongly on Z_s^{sub} when the film is normal. The value of the effective sub-

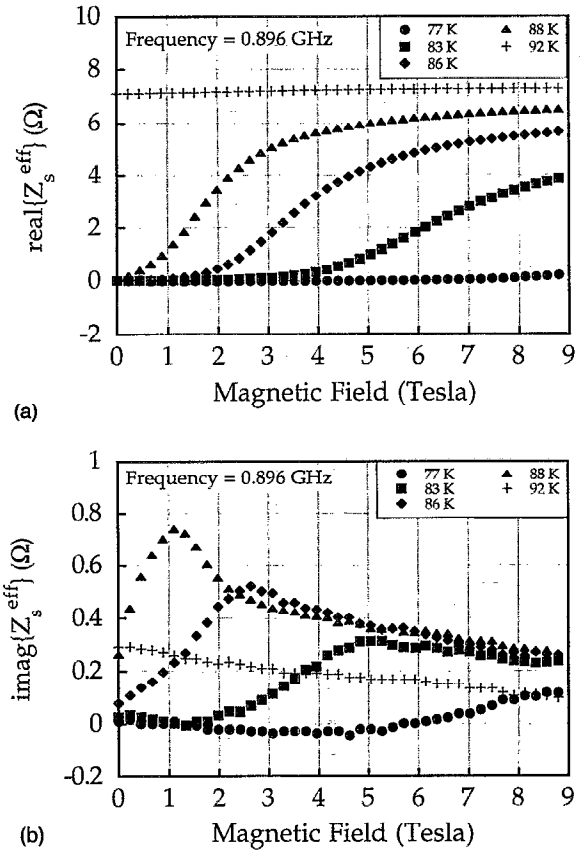

FIG. 4. Magnetic field dependence of the (a) real and (b) imaginary parts of Z_s^{eff} of a 1000 Å YBCO film at various temperatures at 0.896 GHz.

strate impedance obtained from the fit shown in Fig. 3 is: real$\{Z_s^{\text{sub}}\} = 0$, imag$\{Z_s^{\text{sub}}\}=256\ \Omega$.

B. Magnetic field dependence

Having shown that our measurement technique yields reasonable results for the temperature dependence of a YBCO film in zero magnetic field, we would like to apply it to study the effects of vortex motion in similar YBCO samples. The magnetic field dependence of real and imaginary Z_s^{eff} for a 1000 Å YBCO film is shown in Figs. 4(a) and 4(b) for several different temperatures at 0.896 GHz. The effective surface impedance is calculated by a procedure analogous to that used for the temperature dependent data; however, the reference state used for the calculation of E_R is the $B=0$ point at the temperature at which the field sweep is performed [the numerical value of $Z_s(T,B=0)$ necessary for this calibration is taken directly from Figs. 3(a) and 3(b)]. Similar measurements are performed at many different frequencies in the range 45 MHz–20 GHz, which allows us to obtain a more complete picture of how vortices respond to externally applied fields and currents as a function of temperature, magnetic field, and frequency.

Figure 4(a) shows that the real part of the effective surface impedance exhibits a smooth transition from a low-loss regime where vortices are effectively pinned to a de-pinned, lossy regime as a function of magnetic field for all but the lowest and highest temperatures shown. Such a cross-over in the field dependence of the surface resistance has been observed by Sridhar *et al.*[30] in cavity measurements of YBCO films performed at a single frequency. Our results are consistent with theirs; furthermore we find that the field at which this transition occurs depends on not only temperature, but also on frequency. Also, from Fig. 4(a) one can observe at higher temperatures a high-field plateau, which indicates that we have surpassed H_{c2} and driven the film into the normal state.

The corresponding magnetic field dependence of the imaginary part of Z_s^{eff} is shown in Fig. 4(b), and exhibits a pronounced peak at higher temperatures, which is also both temperature and frequency dependent.[31] Both the real and imaginary parts of the magnetic field dependence of Z_s^{eff} are consistent with the unified theory of Coffey and Clem.[2] Detailed analysis of the magnetic field dependence of Z_s^{eff} within the context of the model allows for the evaluation of several vortex motion related parameters, such as the vortex viscosity coefficient η, the pinning force constant κ_p, and the thermal activation barrier U_0 at different temperatures and frequencies. These results will be discussed further in other publications.[31]

C. Frequency dependence

Our magnetic field dependent measurements suggest that the response of vortices to a driving field is different for different frequencies. The frequency dependence of vortex motion can be exclusively explored using our measurement because of the unique ability of the technique to measure the continuous frequency dependence of Z_s^{eff}directly in the rf and microwave regime (45 MHz–20 GHz). As an example, we show in Figs. 5(a) and 5(b) the real and imaginary parts of Z_s^{eff} vs frequency for a 1000 Å YBCO film in zero dc magnetic field at several different temperatures. As with the temperature and magnetic field dependent data, the frequency dependence of Z_s^{eff} shown here is obtained by using the data obtained at 70 K as a reference state, in order to calculate the error coefficient E_R as described in Sec. IV B.

Figure 5(a) shows that by 85 K, the real part of Z_s^{eff} has acquired a significant frequency dependence while the film is still in the superconducting state. The increased losses at higher frequencies are caused by small regions in the film which have been driven normal, as the film has a very broad superconducting transition centered at approximately 89 K. By 92 K, the film is completely in the normal state, and the magnitude of the effective surface resistance has increased dramatically, and only a weak frequency dependence remains, which is most likely due entirely to the effect of radiation leakage into the substrate. One would expect on the basis of Eq. (6) that Z_s^{eff} is independent of frequency in the normal state since $\tilde{\rho}/t_0$ contains no frequency dependence. However, the Z_s^{sub} term in the denominator of Eq. (9) is finite and is also frequency dependent for most practical systems, which gives rise to the observed frequency dependence of the real part of Z_s^{eff}.

Figure 5(b) shows the frequency dependence of the imaginary part of Z_s^{eff}, which is strongly linear at 80 and 85 K. The linear frequency dependence of imag$\{Z_s^{\text{eff}}\}$ is due to the fact that at these temperatures, the effective surface im-

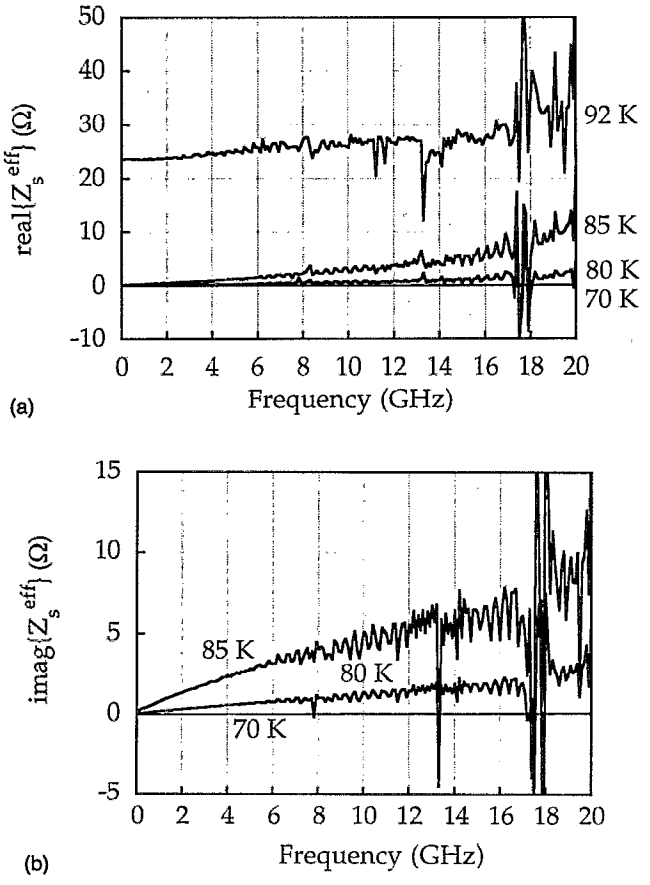

FIG. 5. Frequency dependence of the (a) real and (b) imaginary parts of Z_s^{eff} for a YBCO film at various temperatures in zero magnetic field. The 70 K data is used as a reference state to calibrate the system.

pedance is dominated by the kinetic inductance of the film ($Z_s^{\text{eff}} \approx i\omega L_{\text{kin}}$), which is proportional to λ^2/t_0 in the thin film limit. At temperatures above T_c, where $\tilde{\rho}/t_0$ is completely real, Eq. (10) predicts that the imaginary part of Z_s^{eff} is entirely due to the influence of Z_s^{sub}; it is therefore not shown in Fig. 5(b).

We have verified that the frequency dependence of a YBCO film in zero external magnetic field is consistent with our expectations based on the analysis presented here. Similar measurements performed in the presence of an external field can yield much valuable information about the frequency dependence of vortex dynamics in the rf and microwave regime. The results of such measurements in a magnetic field will also be the subject of future publications.[31]

VI. DISCUSSION

We have presented a method by which both the real and imaginary parts of the surface impedance of superconductors (or other samples) can be measured over a broad range of temperature, magnetic field, and frequency in the rf and microwave regimes. The measurement is particularly well suited for studying the mixed state of type II superconductors, for which it was developed. Experiments on YBCO thin films in zero external magnetic field confirm that the technique can provide an accurate measurement of the effective surface impedance of superconductors in the temperature range near T_c, and similar measurements on YBCO films in the presence of an external magnetic field illustrate the usefulness of the technique for exploring the behavior of vortices in superconductors.

ACKNOWLEDGMENTS

The authors would like to acknowledge Dr. Nathan Bluzer of Westinghouse Advanced Technology Laboratory, Baltimore for assistance in the design of our probe and for many useful discussions, Dr. R. C. Taber of HP Labs for a critical reading of the manuscript, and A. T. Findikoglu for assistance in sample preparation. This work was supported by NSF NYI:DMR-9258183 and NSF DMR-9123198, as well as the State of Maryland.

[1] J. I. Gittleman and B. Rosenblum, Phys. Rev. Lett. **16**, 734 (1966).
[2] M. W. Coffey and J. R. Clem, Phys. Rev. Lett. **67**, 386 (1991).
[3] T. C. Hsu, Physica C **213**, 305 (1993).
[4] D. S. Fisher, M. P. A. Fisher, and D. A. Huse, Phys. Rev. B **43**, 130 (1991).
[5] J. le G. Gilchrist and P. Monceau, J. Phys. C **3**, 1399 (1970).
[6] R. J. Pedersen, Y. B. Kim, and R. S. Thompson, Phys. Rev. B **7**, 982 (1973).
[7] M. Pambianchi, D. H. Wu, L. Ganapathi, and S. M. Anlage, IEEE Trans. Appl. Supercon. **3**, 1425 (1993).
[8] D. A. Soderman and K. Rose, J. Appl. Phys. **39**, 2610 (1968).
[9] E. K. Moser, W. J. Tomasch, J. K. Furdyna, M. W. Coffey, and J. R. Clem, IEEE Trans. Appl. Supercon. **3**, 1119 (1993).
[10] E. K. Moser, W. J. Tomasch, M. J. McClorey, J. K. Furdyna, M. W. Coffey, C. L. Pettiette-Hall, and S. M. Schwarzbek, Phys. Rev. B **49**, 4199 (1994).
[11] H. K. Olsson, R. H. Koch, W. Eidelloth, and R. P. Robertazzi, Phys. Rev. Lett. **66**, 2661 (1991).
[12] N.-C. Yeh, D. S. Reed, W. Jiang, U. Kriplani, F. Holtzberg, A. Gupta, B. D. Hunt, R. P. Vasquez, M. C. Foote, and L. Bajuk, Phys. Rev. B **45**, 5654 (1992).
[13] H. Wu, N. P. Ong, and Y. Q. Li, Phys. Rev. Lett. **71**, 2642 (1993).
[14] O. M. Corbino, Nuovo Cimento **1** (1911); R. P. Heubner, *Magnetic Flux Structures in Superconductors* (Springer, Berlin, 1979), p. 128.
[15] M. P. Shaw and P. R. Solomon, Phys. Rev. **164**, 535 (1967).
[16] N. Bluzer, D. K. Fork, T. H. Geballe, M. R. Beasley, M. Y. Reizer, S. R. Greenfield, J. J. Stankus, and M. Fayer, IEEE Trans. Magn. **27**, 1519 (1991); N. Bluzer, J. Appl. Phys. **71**, 1336 (1992).
[17] Yan-Zhen Wei and S. Sridhar, Rev. Sci. Instrum. **60**, 3041 (1989).
[18] L. L. Li, N. H. Ismail, L. S. Taylor, and C. C. Davis, IEEE Trans. Biomed. Eng. **39**, 49 (1992).
[19] N.-E. Belhadj-Tahar, A. Fourrier-Lamar, and H. DeChanterac, IEEE Trans. Microwave Theory Tech. **38**, 1 (1990).
[20] M. A. Saed, S. M. Riad, and W. A. Davis, IEEE Trans. Microwave Theory Tech. **39**, 485 (1990).
[21] The microwave connector used is a V101-F connector, made by Wiltron Corp.
[22] The coaxial cable used is ISOCORE semi-rigid coaxial cable, manufactured by Rogers Corp., part number IA-086NS.
[23] The scale factor Γ may be obtained from the following considerations. Assume that we have an ideal, lossless coaxial transmission line of inner radius a and outer radius b. For a given (instantaneous) current I flowing through the transmission line, the (instantaneous) magnetic field at a distance r from the transmission line axis is given by $H_\phi = I/2\pi r$ A/m. Similarly, the (instantaneous) electric field generated by an (instantaneous) potential difference V between the inner and outer conductors is given by $E_r = V/[\ln(b/a)r]$ V/m. The ratio V/I in terms of E_r and H_ϕ is given by $V/I = [\ln(b/a)/2\pi](E_r/H_\phi)$. This gives the relationship between the field impedance Z_{field} and the "ohmic" impedance Z_{IV} for the TEM mode in the coaxial system, and yields $\Gamma = \ln(b/a)/2\pi$.
[24] N. Klein, H. Chaloupka, G. Muller, S. Orbach, H. Piel, B. Roas, L. Schultz, U. Klein, and M. Peiniger, J. Appl. Phys. **67**, 6940 (1990).
[25] L. Drabeck, K. Holczer, G. Gruner, and D. Scalapino, J. Appl. Phys. **68**, 892 (1990).
[26] P. Hartemann, IEEE Trans. Appl. Supercon. **2**, 228 (1992).
[27] See, for example, Hewlett Packard Application Note 183, p. 39 (1978).

[28] It should be noted that only the termination connector and a one meter long section of the coaxial cable are cold during the measurement. The remaining connectors in the system all remain at room temperature. In addition, although the error coefficients depend strongly on frequency, we expect them to be only very weakly dependent, if at all, on the temperature, external magnetic field, dc bias current and rf power, at least over the range of the measurements presented here.

[29] The analysis involving TEM waves is actually not appropriate when considering the substrate in the measurement configuration used here because such an analysis assumes the same transverse field variations in the substrate as in the coaxial cable. This is clearly not the case, owing to the different geometries for the substrate and coaxial cable. A more complete calculation must take into account non-TEM propagation in the substrate and coaxial cable, along the lines of Ref. 18. The TEM calculations do, however, give a good indication of the effect of the substrate on our measurement.

[30] J. Owliaei, S. Sridhar, and J. Talvacchio, Phys. Rev. Lett. **69**, 3366 (1992).

[31] J. C. Booth, D. H. Wu, and S. M. Anlage (unpublished).